

## Structure and Mechanisms of South Indian Ocean Climate Variability\*

SHANG-PING XIE<sup>†</sup> AND H. ANNAMALAI

*International Pacific Research Center, University of Hawaii at Manoa, Honolulu, Hawaii*

FRIEDRICH A. SCHOTT

*Institut für Meereskunde, University of Kiel, Kiel, Germany*

JULIAN P. MCCREARY JR.

*International Pacific Research Center and Department of Oceanography, University of Hawaii at Manoa, Honolulu, Hawaii*

(Manuscript received 29 August 2001, in final form 22 October 2001)

### ABSTRACT

A unique open-ocean upwelling exists in the tropical South Indian Ocean (SIO), a result of the negative wind curl between the southeasterly trades and equatorial westerlies, raising the thermocline in the west. Analysis of in situ measurements and a model-assimilated dataset reveals a strong influence of subsurface thermocline variability on sea surface temperature (SST) in this upwelling zone. El Niño–Southern Oscillation (ENSO) is found to be the dominant forcing for the SIO thermocline variability, with SST variability off Sumatra, Indonesia, also making a significant contribution. When either an El Niño or Sumatra cooling event takes place, anomalous easterlies appear in the equatorial Indian Ocean, forcing a westward-propagating downwelling Rossby wave in the SIO. In phase with this dynamic Rossby wave, there is a pronounced copropagation of SST. Moreover, a positive precipitation anomaly is found over, or just to the south of, the Rossby wave–induced positive SST anomaly, resulting in a cyclonic circulation in the surface wind field that appears to feedback onto the SST anomaly. Finally, this downwelling Rossby wave also increases tropical cyclone activity in the SIO through its SST effect.

This coupled Rossby wave thus offers potential predictability for SST and tropical cyclones in the western SIO. These results suggest that models that allow for the existence of upwelling and Rossby wave dynamics will have better seasonal forecasts than ones that use a slab ocean mixed layer. The lagged-correlation analysis shows that SST anomalies off Java, Indonesia, tend to precede those off Sumatra by a season, a time lead that may further increase the Indian Ocean predictability.

### 1. Introduction

The El Niño–Southern Oscillation (ENSO) in the equatorial Pacific exerts a strong influence on the global climate (Wallace et al. 1998; Trenberth et al. 1998; Slingo and Annamalai 2000). During El Niño, the center of atmospheric deep convection shifts from Indonesia to the central equatorial Pacific, reducing the convection in the equatorial Indian and western Pacific. This shift in convection drives anomalous westerly winds, pro-

viding positive feedback onto the anomalously high sea surface temperatures (SSTs) in the eastern Pacific (Bjerknes 1969). In the Indian Ocean, the response includes anomalous easterly winds near the equator that are followed by a basinwide warming (Nigam and Shen 1993; Klein et al. 1999; Lau and Nath 2000).

The Indian Ocean is the only tropical ocean where the annual-mean winds on the equator are westerly. As a result of weak winds, the equatorial thermocline is flat and deep (Fig. 1). Such an annual-mean climatology—deep thermocline and absence of equatorial upwelling—limits the effect of thermocline depth variability on SST, a key element to the Bjerknes feedback, leading to a view that the Indian Ocean cannot develop its own interannual variability and thus has to follow Pacific ENSO rather passively (e.g., Latif and Barnett 1995). Occasionally, however, the Indian Ocean develops an equatorial cold tongue for a period of a few months (Saji et al. 1999; Webster et al. 1999; Yu and Rienecker 1999; Murtugudde et al. 2000; Ueda and Mat-

\* International Pacific Research Center Contribution Number 121 and School of Ocean and Earth Science and Technology Contribution Number 5881.

<sup>†</sup> Additional affiliation: Department of Meteorology, University of Hawaii at Manoa, Honolulu, Hawaii.

*Corresponding author address:* Dr. Shang-Ping Xie, International Pacific Research Center, SOEST, University of Hawaii at Manoa, 2525 Correa Rd., Honolulu, HI 96822.  
E-mail: xie@soest.hawaii.edu

sumoto 2000), with atmospheric convection, wind, thermocline depth, and SST covarying in a manner consistent with the positive-feedback loop Bjerknes (1969) suggested for the Pacific. This unstable development of cold SSTs in the eastern equatorial Indian Ocean seems to result from anomalous seasonal upwelling off Sumatra, Indonesia. Such Sumatra cooling events do not always occur in concert with the Pacific El Niño events (Reverdin et al. 1986; Meyers 1996; Saji et al. 1999; Webster et al. 1999), thereby providing a mechanism for the Indian Ocean–atmosphere to develop its own variability independent of ENSO.

There is observational evidence that SST variability in some parts of the Indian Ocean cannot be modeled by a passive, vertically one-dimensional slab mixed layer. In an analysis of observational data for 1952–92, Klein et al. (1999) report that surface heat flux anomalies explain the ENSO-induced basinwide warming over most of the tropical Indian Ocean, but identify the western tropical South Indian Ocean (SIO) as an exception, suggesting that some yet unidentified mechanisms are at work there. Lau and Nath (2000) force an atmospheric general circulation model (AGCM) with the observed time evolution of SST in the tropical Pacific, while allowing SST elsewhere to interact with the atmosphere according to a slab mixed layer model. ENSO-based composite SST anomalies in this partially coupled model resemble observations in the North Indian Ocean, but are weak and sometimes have opposite signs to observations in the equatorial and tropical South Indian Ocean [see also Alexander et al. (2001, manuscript submitted to *J. Climate*, hereafter ABNLLS) for a simulation with a larger ensemble size]. Thus, Lau and Nath's (2000) model results are consistent with those of Klein et al. (1999), and together these studies suggest that mechanisms other than ENSO-induced changes in surface heat flux influence interannual SST variability in the tropical SIO. Consistent with these atmospheric studies, ocean model results (Murtugudde and Busalacchi 1999; Murtugudde et al. 2000; Behera et al. 2000; Huang and Kinter 2001) and empirical analysis of satellite sea surface height (SSH) measurements (Chambers et al. 1999) suggest that ocean dynamic processes contribute to SST variability in the western SIO.

In the present study, we investigate the mechanisms for SIO climate variability using model-assimilated datasets and in situ/satellite measurements. While previous studies of SIO variability tend to focus either on atmospheric or oceanic aspects of the problem, here we attempt to construct a physically consistent scenario that links various phenomena from a coupled ocean–atmosphere interaction perspective. Of particular interest to us is how subsurface-ocean wave processes can affect SST, since they carry the memory of wind forcing in the past and provide potential predictability. Toward this end, we analyze a three-dimensional ocean dataset derived from model-data assimilation (Carton et al. 2000). Key questions to be investigated are how the ocean

mean state sets the stage for subsurface processes to affect SST; what is the atmospheric forcing for subsurface anomalies; and whether such anomalies exert any significant effect on the atmosphere. Related to the second question, we will assess the relative importance of the forcing by ENSO and Sumatra variability in light of the recent advances in the Indian Ocean climate research.

Our major conclusion is that much of SST variability in the western tropical SIO (up to 50% of the total variance in certain seasons) is not locally forced but is instead due to oceanic Rossby waves that propagate from the east. We will show that ENSO is the major forcing for these Rossby waves and that they interact with the atmosphere after reaching the western ocean. Such a subsurface effect on SST in the western tropical SIO is made possible by the simultaneous presence of upwelling and a shallow thermocline.

The paper is organized as follows. Section 2 introduces the datasets. Section 3 describes the mean state of the Indian Ocean climate, identifies regions where the subsurface ocean has a significant influence on SST, and relates the subsurface variability to ocean Rossby waves. Sections 4 and 5 examine the forcing for these Rossby waves and how they interact with the atmosphere, respectively. Section 6 discusses interannual variability in other parts of the SIO. Section 7 is a summary and discusses the implications of this study.

## 2. Data

Hydrographic measurements in the open oceans are generally sparsely and unevenly distributed in space and time. In the late 1980s and since 1992, satellite altimetry measurements have greatly enhanced our ability to infer thermocline variability on meso- to interannual timescales. Carton et al. (2000) use an ocean general circulation model to interpolate unevenly distributed ocean measurements into three-dimensional global fields of temperature, salinity, and current velocity. This simple ocean data assimilation (SODA) product will be the primary dataset for the following analysis. It is available at  $1^\circ \times 1^\circ$  resolution in the midlatitudes and  $0.45^\circ \times 1^\circ$  latitude–longitude resolution in the Tropics, and has 20 vertical levels with 15-m resolution near the sea surface. While such model-assimilated products will improve with time as more data become available and assimilation technique advances, we feel that SODA is a reasonable representation of the history of the tropical oceans, where wave dynamics is a major mechanism for subsurface variability and even forward models give decent simulations when forced by observed winds (e.g., Murtugudde et al. 2000; Behera et al. 2000). We will analyze SODA for 1970–99, a period when the use of expendable bathythermograph (XBT) and conductivity–temperature–depth (CTD) sensors became widespread worldwide, resulting in a great increase in the number of measurements below 200 m (Carton et al. 2000). An

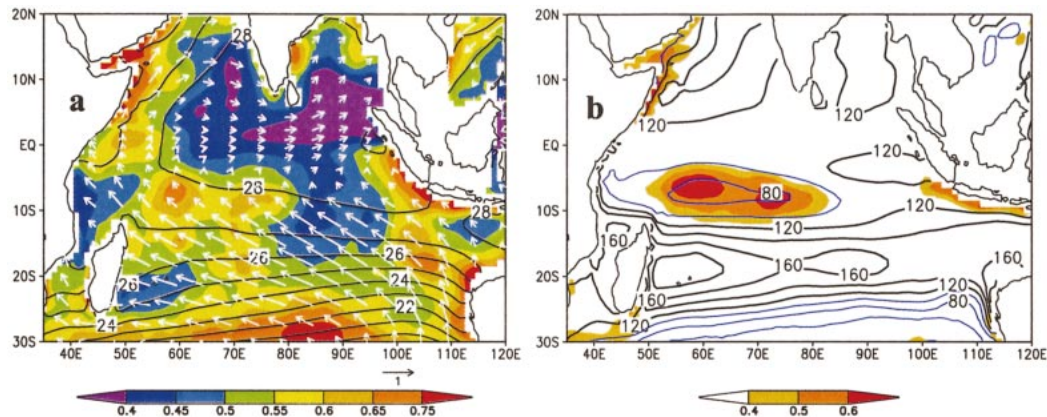


FIG. 1. Annual-mean distributions of (a) wind stress (vectors in  $\text{N m}^{-2}$ ), SST (contours in  $^{\circ}\text{C}$ ) and its interannual rms variance (color shade); and (b) the  $20^{\circ}\text{C}$  isothermal depth (contours in m) and its correlation with local SST anomalies (color shade).

analysis using a longer record for 1950–99 gives qualitatively the same results.

We use a repeated XBT line [the World Ocean Circulation Experiment (WOCE) IX-12] that began in 1986 and runs from the northwestern ( $11.3^{\circ}\text{N}$ ,  $52.3^{\circ}\text{E}$ ) to southeastern ( $31.7^{\circ}\text{S}$ ,  $114.9^{\circ}\text{E}$ ) Indian Ocean (Masumoto and Meyers 1998). It should be noted that the IX-12 line is not exactly repeated and individual observation stations spread in longitude by up to  $10^{\circ}$  in the SIO (Pigot and Meyers 1999). In an analysis to be presented in section 3, SODA compares very well with the in situ XBT measurements and is capable of producing a smooth transition across the XBT line, an indication that the assimilation is not overfitted to observations. SODA further compares quite well with the TOPEX/Poseidon (T/P) sea surface height measurements available since 1993 (not shown). We also compared the SODA SST with the satellite-in situ blended dataset (Reynolds and Smith 1994) that are available since 1982, and the two datasets give similar results over the overlapping period (not shown).

To study the interaction with the atmosphere, we use wind stress based on the Comprehensive Ocean–Atmosphere Data Set (COADS; da Silva et al. 1994) for 1950–92 and the National Centers for Environmental Prediction–National Center for Atmospheric Prediction (NCEP–NCAR) reanalysis (Kalnay et al. 1996) after 1993, the same data that are used as the surface forcing for SODA. To better resolve coastal winds, we use the 8-yr (1992–99) climatology of the wind stress measurements by the European Remote Sensing (ERS) satellites. In the Tropics, surface winds and deep convection are generally tightly coupled. This study uses monthly precipitation anomalies derived from the Climate Prediction Center (CPC) Merged Analysis of Precipitation (CMAP) dataset for 1979–99 (Xie and Arkin 1996). To study severe weather disturbances, days of named tropical storms/cyclones on a  $4^{\circ}$  latitude  $\times$   $5^{\circ}$

longitude grid are determined from a cyclone track dataset for 1951–98 (Mitchell 2001).

In our analysis, the monthly mean climatology is first calculated for the study period. Then, interannual anomalies are computed as the difference from this climatology. Unless stated otherwise, we use SODA SST and thermocline depth and the merged COADS–NCEP wind stress in the following analysis.

### 3. Thermocline feedback in the western tropical SIO

In the tropical oceans, wind-induced upwelling combined with a shallow thermocline often causes a local minimum in climatological SST. In the presence of upwelling, a change in the thermocline depth  $\Delta h$  can lead to a SST anomaly that may not correlate with local atmospheric forcing. This “thermocline feedback” on SST is at the heart of ENSO, where it manifests itself as a SST variance maximum that extends from the coast of South America far into the west along the equator. We emphasize that upwelling alone may not be sufficient for this thermocline feedback to operate. For example, near the international date line easterly winds maintain equatorial upwelling, but this thermocline feedback is only of secondary importance (Schiller et al. 2000) because the thermocline there is deep ( $\sim 160$  m). Thus, both upwelling and a shallow thermocline are necessary conditions for this thermocline feedback (e.g., Neelin et al. 1998; Xie et al. 1989). In this section, we first demonstrate that thermocline feedback is active in the western tropical SIO. Generally, we use the  $20^{\circ}\text{C}$  isothermal depth ( $Z_{20}$  hereafter) as a proxy for thermocline depth. Then, we show that  $\Delta h$  there is remotely forced by Rossby waves from the east.

#### a. Covariability of SST and thermocline depth

Figure 1 shows the root-mean-square (rms) variance of interannual SST variability along with the annual-

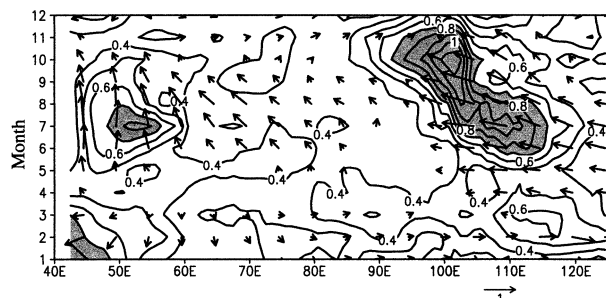


FIG. 2. Distance–time section of climatological wind stress vectors ( $\text{N m}^{-2}$ ) and rms interannual variance of SST (contours; shade  $> 0.7^\circ\text{C}$ ) along the equator up to  $97^\circ\text{E}$  and then southeastward along the Indonesia coast. The along- (across) shore/equator wind component appears as horizontal (vertical). SST is based on the satellite/in situ blended product for 1982–2000 and wind on *ERS* scatterometer measurements for 1992–99.

mean SST and surface winds stress. Note that there is not a SST variance maximum along the equator. Under the weak equatorial westerlies, the thermocline is nearly flat at 120 m along the equator. The westerlies, together with the deep thermocline, suppress thermocline feedback on equatorial SST, responsible for the absence of a variance maximum there.

During the Asian summer monsoon season, strong coastal upwelling takes place off Somalia in the west and off Indonesia in the east, causing a local SST variance maximum in each of these upwelling sites in Fig. 1. Figure 2 gives a detailed view of the Indonesian maximum, showing rms SST variance on a space coordinate that follows the west coast of Indonesia up to  $97^\circ\text{E}$  and then coincides with the equator. Alongshore winds start to increase in April and then intensify probably in response to the northward migration of the sun and atmospheric deep convection. These alongshore southeasterlies induce coastal upwelling, leading to an increase in rms SST variance by a factor of 2. The maximum SST variance first appears on the Java coast, Indonesia, in April and then moves northwestward following the maximum alongshore wind and coastal upwelling. This coastal SST variability extends onto the equator in August. The SST variance peaks off Sumatra and on the equator in October and then decays rapidly.

In the open Indian Ocean, SST variance is notably larger south than north of the equator. Enhanced SST variance is found in the western tropical SIO, from  $5^\circ$  to  $15^\circ\text{S}$  and  $50^\circ$  to  $80^\circ\text{E}$ . In contrast to the monsoonal winds in the North Indian Ocean, the southeasterly trade winds are present throughout the year in the SIO. Annual-mean southeasterly wind speed peaks between  $15^\circ$  and  $20^\circ\text{S}$ , and the curl between the southeasterly trades and equatorial westerlies implies that an upwelling zone is present from  $5^\circ$  to  $15^\circ\text{S}$  year-round. To the lowest order, the wind curl is zonally uniform, which drives a cyclonic equatorial gyre with the thermocline shoaling westward (e.g., Schott and McCreary 2001). The Z20 minimum is about 70 m at  $8^\circ\text{S}$ ,  $60^\circ\text{E}$ , a depth observed

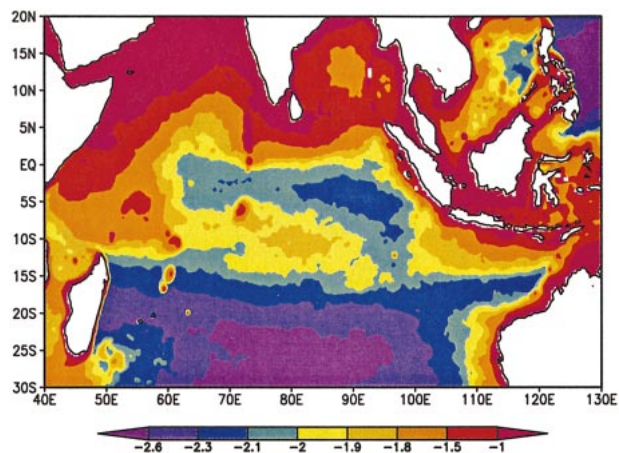


FIG. 3. Natural logarithm of 1998–2000 mean chlorophyll concentration ( $\text{mg m}^{-3}$ ) measured by the SeaWiFS satellite.

at  $120^\circ\text{W}$  in the equatorial eastern Pacific. Unlike other major upwelling zones, the western SIO upwelling does not lead to a local SST minimum in the annual-mean SST, presumably because it is relatively weak and its effect is masked by an equatorward SST gradient. It does, however, reveal itself as a meridional maximum in chlorophyll concentration measured by the Sea-viewing Wide Field-of-View Sensor (SeaWiFS) satellite (Fig. 3; see also Murtugudde et al. 1999).

To measure the thermocline feedback more exactly, we compute the correlation between interannual variability in Z20 and SST,  $r(z, \text{SST})$ . We note that this correlation probably underestimates the real subsurface effects, as it measures only the local effect of subsurface variability through upwelling/entrainment and may not properly account for horizontal advection by anomalous currents associated with thermocline variability. As expected, high  $r(z, \text{SST})$  values are found in the seasonal upwelling zones off Somalia and Indonesia (Fig. 1b). In addition, high correlation appears in the western SIO, collocated both with the shallow thermocline and the local SST variance maximum. We conclude that this open-ocean upwelling allows thermocline variability to enhance SST variability where the thermocline is shallow.

We have made the same correlation analysis using satellite SSH and SST measurements for October 1992–December 1999, a period when both are available. The SODA- and satellite-based results are similar. In particular, the high  $r(z, \text{SST})$  correlations in the SIO open-ocean upwelling and Sumatra coastal upwelling zones stand out in both analyses, with a comparable magnitude and spatial distribution.

#### b. Validation with XBT data

Australia's Commonwealth Scientific and Industrial Research Organisation (CSIRO) Marine Research has maintained a repeated XBT line since 1986, which cuts

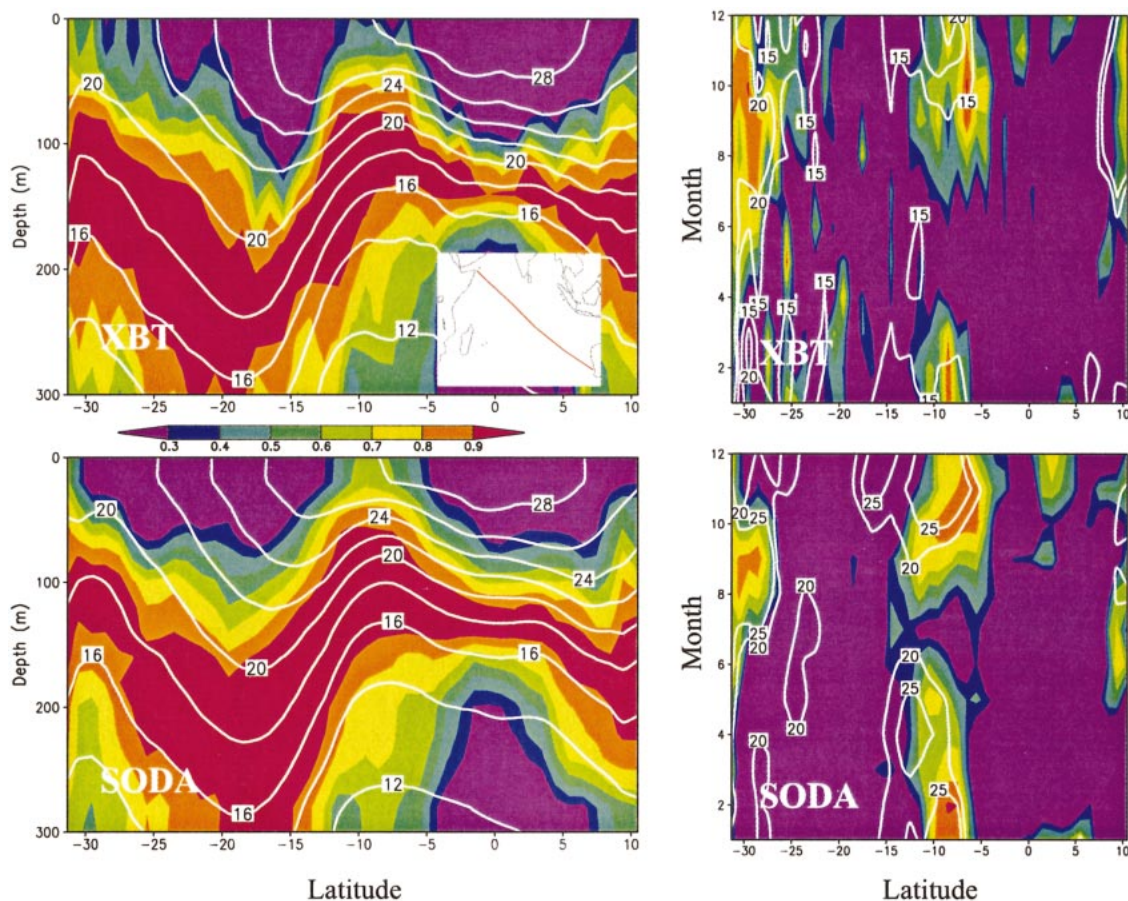


FIG. 4. Temperature correlation (color shade) with interannual variations in the  $18^{\circ}\text{C}$  isothermal depth ( $Z_{18}$ ) of (top) in situ observations and (bottom) SODA along the IX-12 XBT line (inset top left). (left) Annual-mean correlation as a function of lat and depth, along with the mean isothermals (contours in  $^{\circ}\text{C}$ ). (right) Monthly correlation at the sea surface as a function of lat and calendar month, along with the rms variance of  $Z_{18}$  (contours in m). The  $Z_{18}$ -SST correlation tends to be high in the open-ocean upwelling zone  $5^{\circ}$ - $12^{\circ}\text{S}$ . In both in situ observations and SODA, the  $Z_{18}$ -SST correlation is small during Jun-Jul when the interannual variance of the thermocline depth reaches its seasonal minimum.

across the eastern edge of the shallow thermocline region in the western SIO (inset of Fig. 4). From this long-term in situ dataset, we construct a bimonthly climatology and interannual anomalies to assess the strength of thermocline feedback. Since  $Z_{20}$  outcrops in the southern end of this observation line in local winter, the  $18^{\circ}\text{C}$  isothermal ( $Z_{18}$ ) is used instead to track the thermocline.

The upper-left panel of Fig. 4 shows the correlation of ocean temperature with  $Z_{18}$  on this XBT transect. Over most of this transect, the  $Z_{18}$ -temperature correlation is trapped within the thermocline with a vertical structure indicative of the first baroclinic mode. High correlation ( $>0.4$ ) penetrates above the mixed layer and shows a tendency to reach the surface in the  $5^{\circ}$ - $12^{\circ}\text{S}$  band where the thermocline is shallowest. For comparison, we compute the  $Z_{18}$ -temperature correlation for the same period along this transect using SODA. Both the mean thermal structure and the correlation distribution are remarkably similar to those based on XBT

measurements. In SODA, the 0.6 correlation contour reaches all the way to the sea surface at  $10^{\circ}\text{S}$ . Model errors may cause this difference, but it is also possible that high-frequency internal waves and atmospheric weather-induced variability are responsible for the lower  $z$ -SST correlation in the XBT data. Further assimilation experiments are necessary to sort out the cause of this XBT-SODA difference. It is noteworthy that this analysis of interannual variability implies the existence of open-ocean upwelling in the SIO, whereas the annual-mean SST yields no clue to its existence.

The right panels of Fig. 4 display correlations between  $Z_{18}$  and SST as a function of latitude and calendar month. Again, the correlation is generally similar between SODA and observations, but noisier in the XBT data, a difference likely due to sampling. In the  $5^{\circ}$ - $12^{\circ}\text{S}$  upwelling band, the  $Z_{18}$ -SST correlation is high from August to March, with a maximum value exceeding 0.8. It falls close to zero during June and July not because of diminished upwelling, which actually intensifies in

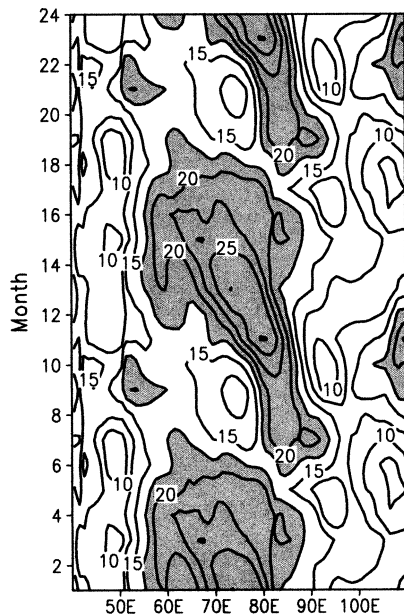


FIG. 5. Rms interannual Z20 variance (shade  $> 17.5$  m) averaged in  $8^{\circ}$ – $12^{\circ}$ S as a function of lon and calendar month.

boreal summer, but rather because of diminished variability in the thermocline depth.

The good agreement of correlation patterns using SODA and XBT observations gives us confidence in the realism of SODA. This resemblance is not too surprising, but overfitting the model to data can result in discontinuities across the XBT line. Such discontinuities are not observed in SODA as the next section will show.

### c. Rossby wave

We turn our attention to the cause of thermocline variability in the western tropical SIO. Figure 5 displays the rms variance of interannual Z20 anomalies along  $10^{\circ}$ S as a function of longitude and calendar month. Thermocline variability is strongly phase locked to the seasonal cycle, growing rapidly from September to November at  $82^{\circ}$ E and thereafter showing a tendency for westward propagation.

To illustrate the time–space evolution of thermocline variability in the SIO, we cross-correlate Z20 variability along  $10^{\circ}$ S with the interannual time series of December Z20 anomalies averaged in  $8^{\circ}$ – $12^{\circ}$ S,  $75^{\circ}$ – $85^{\circ}$ E. A distinct westward propagation emerges (Fig. 6a). The correlation maximum that begins at  $90^{\circ}$ E in June reaches  $57^{\circ}$ E in May of the following year. Such westward-propagating thermocline-depth anomalies have been studied using in situ/satellite measurements and ocean models and attributed to oceanic Rossby waves (Perigaud and Delecluse 1993; Masumoto and Meyers 1998; Chambers et al. 1999; Birol and Morrow 2001). While the westward phase propagation of thermocline anomalies along  $10^{\circ}$ S is expected from ocean hydrodynamics,

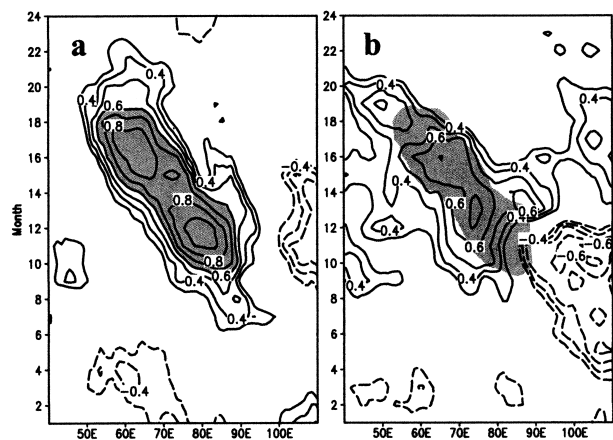


FIG. 6. Lagged correlations of (a) Z20 and (b) SST, averaged in  $8^{\circ}$ – $12^{\circ}$ S, with the Dec Z20 averaged in  $75^{\circ}$ – $85^{\circ}$ E as a function of lon and calendar month. In (b), the Z20 correlation is repeated in shade ( $r > 0.6$ ).

it is rather surprising to see a westward copropagation in SST correlation (Fig. 6b). Westward phase propagation of SST anomalies is especially pronounced west of  $70^{\circ}$ E after February of the following year and can be traced until August to  $40^{\circ}$ E. With local anomalous winds being quite weak (section 4b), the subsurface Rossby wave is the most likely cause of westward-moving SST anomalies.

The tendency for westward propagation of SST anomalies along  $10^{\circ}$ S can be seen even in the raw satellite–in situ blended SST data. Figure 7 shows SST anomalies averaged in  $8^{\circ}$ – $12^{\circ}$ S for 1997–99. A warm anomaly first appears at  $95^{\circ}$ E in May 1997, then travels to the west and can be traced to  $55^{\circ}$ E in July 1998. As this positive anomaly dissipates in the west, a negative SST anomaly emerges at  $85^{\circ}$ E and moves westward. It somehow disappears in February 1998 but reemerges again in March and persists for another few months. A positive SST anomaly, though much weaker, surfaces at  $85^{\circ}$ E in July 1999 and moves westward. So it appears that the westward-traveling tendency in SODA SST is indeed real. There are, however, other features in Fig. 7 unrelated to the Rossby wave mechanism. For example, the eastern tropical SIO tends to develop SST anomalies of the same sign as in the west around April, a tendency visible in Fig. 6b and possibly related to ENSO (see section 4b and Fig. 11b).

## 4. Remote forcing

The strong seasonality in the SIO Rossby wave offers a valuable clue to its forcing mechanism. As SIO thermocline-depth variability appears to be governed by linear wave dynamics (Masumoto and Meyers 1998), it is reasonable to assume that its forcing is also highly seasonally phase locked. Here, we study two possible mechanisms for forcing the wave; namely, Pacific ENSO and Sumatra SST variability.

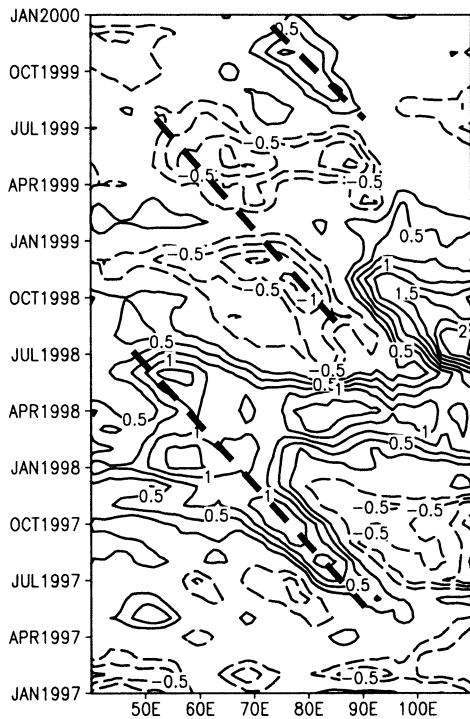


FIG. 7. Longitude–time section of blended satellite–in situ SST ( $^{\circ}\text{C}$ ) averaged in  $8^{\circ}$ – $12^{\circ}\text{S}$  during 1997–99. The long dashed line denotes the  $35^{\circ}\text{ yr}^{-1}$  phase line, a phase speed estimated based on Figs. 5 and 6a.

#### a. Indices and correlations

We use SSTs averaged in  $3^{\circ}\text{S}$ – $3^{\circ}\text{N}$ ,  $180^{\circ}$ – $140^{\circ}\text{W}$  to track ENSO in the Pacific and in  $10^{\circ}\text{S}$ – $0^{\circ}$ ,  $90^{\circ}$ – $100^{\circ}\text{E}$  to capture the SST variance maximum in the eastern equatorial Indian Ocean (Fig. 1a). Figure 8 shows the rms variance of these SST indices as a function of calendar month. Both indices show strong seasonal variations. Because of this seasonality, all the correlation/regression analyses in this paper will be carried out with data stratified in calendar month. We choose SST off Sumatra averaged for September–November as a base time series and refer to it as the *Sumatra index*. Similarly, we use the October–December mean SST in the eastern equatorial Pacific to represent ENSO and call it the *ENSO index*. The cross correlation between the Sumatra and ENSO indices is  $-0.57$ , significant above the 95% level. (Because of a relatively long de-correlation timescale, the following results are insensitive to slight changes in the choice of season for ENSO index.)

First, we examine the lagged cross correlation between equatorial SST and wind (averaged for  $3^{\circ}\text{S}$ – $3^{\circ}\text{N}$ ) with the two indices. Figure 9a shows the lagged SST correlation with the Sumatra index along the equator. The decorrelation scale in the eastern Indian Ocean is rather short at less than half a year, so a conservative sample-size estimate is 30, for which a correlation coefficient of 0.36 is the 95% significance level based on a Student's  $t$  test. High correlations are found in the

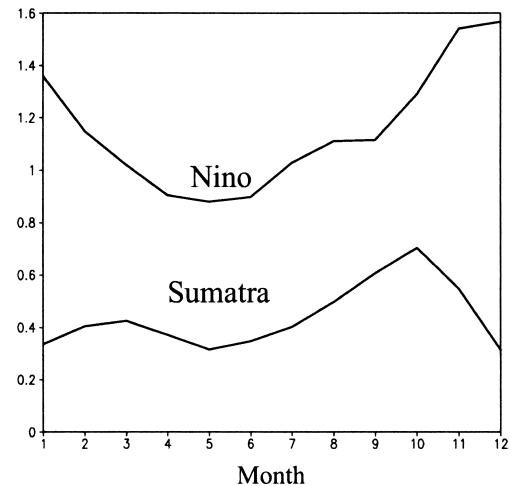


FIG. 8. Rms variance of SST ( $^{\circ}\text{C}$ ) in the eastern equatorial Pacific and Indian Oceans as a function of calendar month.

eastern Indian and Pacific Oceans during the second half of the year. The latter reaches a maximum in October–December.

Figure 9b shows the correlations with the ENSO index, and both the SST and wind patterns are strikingly similar to those in Fig. 9a, albeit higher in the Pacific as expected. In the eastern Pacific, the correlation is rather symmetric before and after the October–December season on which this ENSO index is based. By contrast, the correlation in the Indian Ocean is highly asymmetric, significantly positive following the ENSO. This delay is consistent with the previous results that a basinwide warming takes place in the tropical Indian Ocean following the ENSO (Nigam and Shen 1993; Klein et al. 1999). Note that the positive correlation in the western equatorial Indian Ocean is significantly higher (by 0.2 or more) with the ENSO index than with the Sumatra index.

Only during the second half of the year does coastal upwelling contribute effectively to SST variability off Sumatra (Fig. 2). For the rest of time, Sumatra SST variability is much weaker and caused by different mechanisms. This seasonal change in physical mechanism for Sumatra SST variability has led us to stratify data by calendar month. Without this stratification, the simultaneous correlation of Sumatra SST with other variables vanishes everywhere except in the eastern equatorial Indian Ocean (not shown), a result consistent with Saji et al. (1999). Independent studies using observational data (Tokinaga and Tanimoto 2001, manuscript submitted to *Geophys. Res. Lett.*, hereafter TOTA) and model simulation (Huang and Kinter 2001) also find this correlation between ENSO and Sumatra SST variability. TOTA note a similar sensitivity of the correlation to seasonal stratification and suggest that during a Pacific warm event, anomalous easterlies in the equatorial Indian Ocean can help cool the eastern Indian Ocean.

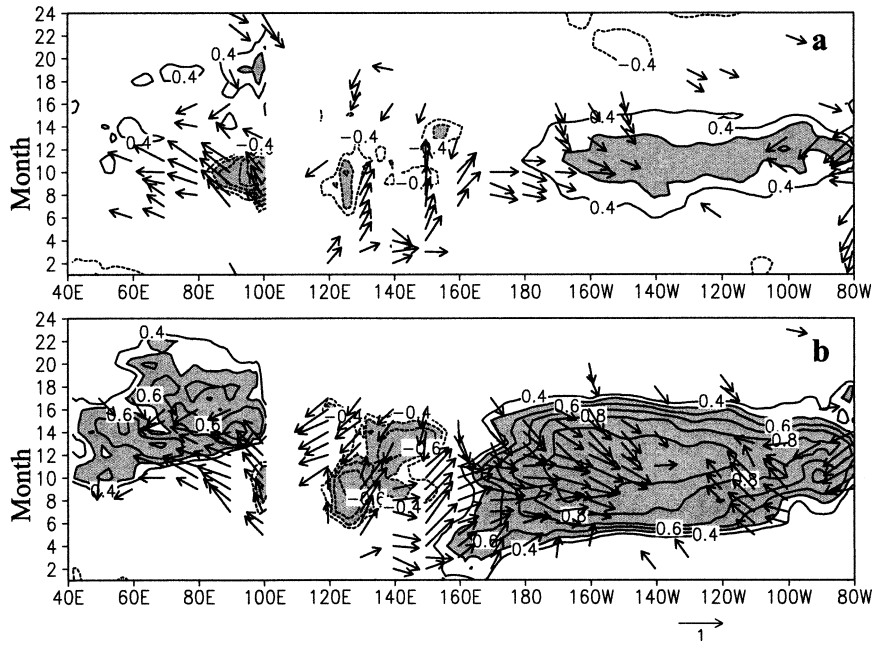


FIG. 9. Lagged correlations of SST (contours;  $|r| > 0.5$  shaded) and surface wind stress (vectors), averaged in  $3^{\circ}\text{S}$ – $3^{\circ}\text{N}$ , with (a) the Sumatra and (b) the ENSO indices. The sign is reversed in (a) to facilitate comparison.

*b. ENSO forcing*

East of  $60^{\circ}\text{E}$ , zonal wind in the equatorial Indian Ocean is highly correlated with our ENSO index (Fig. 9b). Anomalous southeasterlies first appear off Sumatra as early as May and expand to the west progressively with the SST cooling in the eastern Indian Ocean. This close relationship between SST and wind anomalies supports the notion that the development results from a positive feedback (Saji et al. 1999; Webster et al. 1999).

The eastern Indian Ocean cooling dissipates by the following January, but the easterly anomalies persist on the equator until April, suggesting that ENSO forcing is at least a partial cause of these anomalous winds.

The anomalous equatorial easterlies are the major forcing for the SIO Rossby wave. Figure 10 shows the regression coefficients of SST, wind stress, and Z20 with the ENSO index. The SST–wind pattern is very similar to that of Saji et al. (1999) based on an Indian Ocean dipole index, and is indicative of a Bjerknes-type feedback along the equator. In particular, the narrow tongue of cold SST anomalies that penetrate westward along the equator is indicative of equatorial upwelling induced by the easterlies.

The curl associated with these easterlies induces anomalous Ekman downwelling on both sides of the equator, forcing a pair of downwelling equator-trapped Rossby waves that reach the western boundary in December–February (not shown). Webster et al. (1999) and Murtugudde et al. (2000) show that these equatorial Rossby waves cause the delayed warming in the western Indian Ocean after the strong 1997 event of Sumatra cooling. Here, we focus on the Rossby waves farther to the south.

The easterly wind anomalies have a much broader meridional scale south than north of the equator. The associated downwelling forces an off-equatorial Rossby wave with a maximum amplitude at  $10^{\circ}\text{S}$ ,  $80^{\circ}\text{E}$  in October–November (Fig. 10). Figure 11c shows correlation coefficients of the Ekman pumping velocity and Z20, both averaged for  $8^{\circ}$ – $12^{\circ}\text{S}$ , with the ENSO index. Large

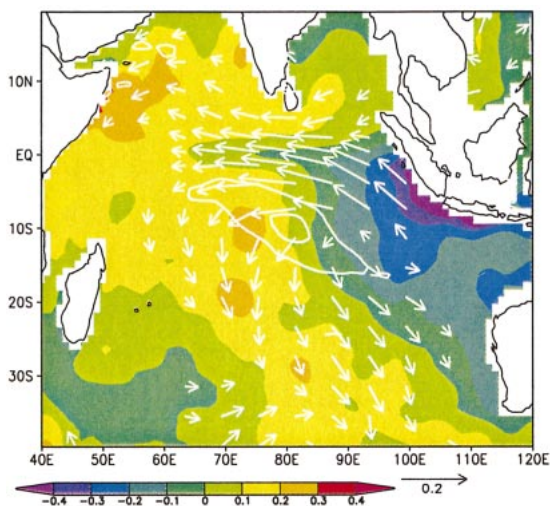


FIG. 10. Regression coefficients of SST (color shade in  $^{\circ}\text{C}$ ), surface wind stress (vectors in  $10^{-1} \text{ N m}^{-2}$ ), and Z20 (contours in 5 and 10 m) in Oct–Nov with the ENSO index. The sign is reversed.

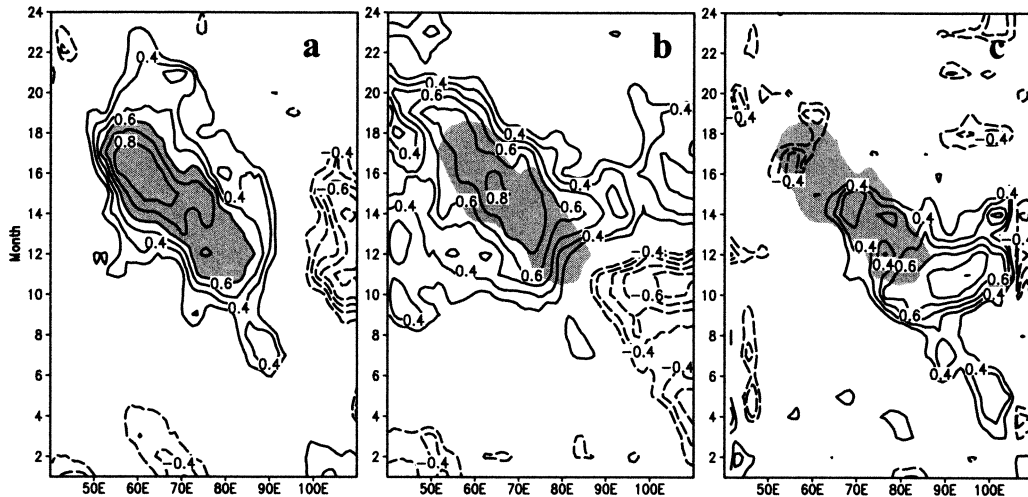


FIG. 11. Lagged correlations of (a) Z20, (b) SST, and (c) Ekman pumping velocity (downward positive), averaged in  $8^{\circ}$ – $12^{\circ}$ S, with the ENSO index as a function of lon and calendar month. The Z20 correlation is replotted in (b) and (c) and shaded ( $r > 0.6$ ).

positive pumping takes place in the eastern half of the basin. The strongest off-equatorial anomalous Ekman pumping occurs during September–December, coinciding with the maximum equatorial easterlies (Fig. 9a). While dampening the negative Rossby waves resulting from the reflection of the upwelling equatorial Kelvin wave, the strong Ekman downwelling excites a downwelling Rossby wave that propagates slowly all the way to the west (Fig. 11a). The Indonesian throughflow enters the Indian Ocean in this latitude band and is an additional mechanism for interannual variability (Godfrey 1996; Birol and Morrow 2001). This effect should be examined in the future with high-resolution datasets that resolve the throughflow.

The SST correlation again shows a distinct westward copropagation with Z20 (Fig. 11b). The SST correlation

with ENSO here is slightly higher (by 0.1) than that with the SIO Z20 in Fig. 6b, but they are otherwise similar in overall pattern. This confirms the Rossby wave as the cause of the SST anomaly and suggests that ENSO is the major forcing for both. Ocean model results support this notion. In simulations where wind-induced interannual variations in surface heat flux are artificially suppressed, SST variance is greatly reduced almost everywhere but remains strong in the western tropical SIO (Murtugudde and Busalacchi 1999; Behera et al. 2000). Murtugudde et al. (2000) find that vertical entrainment, along with meridional advection, is a major contributor to the warming in late 1997 and early 1998 in the western tropical SIO. Since anomalous zonal winds vary their direction over the westward-traveling positive SST anomaly (Fig. 12b), meridional Ekman advection is not a robust forcing for SST. Anomalous meridional winds are more robust and maintain a southward direction as noted by White (2000), but the associated Ekman advection must be small given the weak zonal SST gradient.

While the near-equatorial Rossby waves are found on both sides of the equator, ENSO-forced off-equatorial Rossby waves are pronounced only in the SIO (Fig. 10). The cause of this asymmetry is unclear at this time, but hemispheric asymmetry in atmospheric circulation may be responsible. In addition, Sri Lanka, with its south coast at  $6^{\circ}$ N, is a barrier that blocks the westward propagation of off-equatorial Rossby waves in the North Indian Ocean.

### c. Sumatra forcing

Given the possibility of Bjerknes feedback in the Indian Ocean, an alternative of the above ENSO-forced scenario is that Sumatra SST variability is the primary

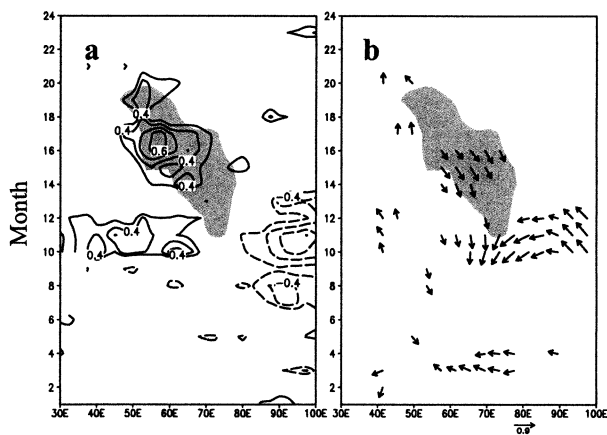


FIG. 12. Lagged correlations of (a) precipitation (contours) and (b) surface wind stress (vectors), averaged in  $8^{\circ}$ – $12^{\circ}$ S, with the ENSO index as a function of lon and calendar month. The SST correlation ( $r > 0.6$ ) is shaded.

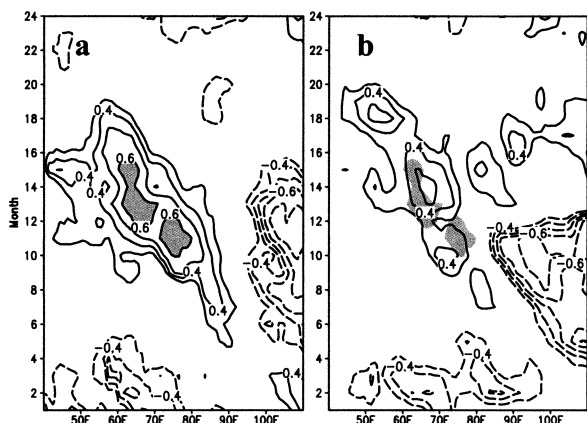


FIG. 13. Same as Fig. 11 except for correlation with the Sumatra index. The sign is reversed to facilitate comparison.

forcing for SIO variability, which was in fact our initial hypothesis. Such a Sumatra-centered scenario is possible at least in a coupled ocean–atmosphere general circulation model, in which Sumatra variability remains strong even without interannual SST variations in the Pacific and Atlantic (J.-Y. Yu and K.-M. Lau 2001, personal communication; see also Iizuka et al. 2000).

Figure 13 shows the lagged correlation of Z20 and SST with the Sumatra index. The overall structure is very similar to that based on the ENSO index, except the correlation coefficients are significantly smaller (by 0.2 for both Z20 and SST). The Sumatra effect is visible even in our ENSO index–based analysis; the westward expansion of the positive Ekman pumping during September–November (Fig. 11c) is probably associated with the coupled westward development of the equatorial cold tongue and easterly winds (Fig. 9b), all of which appear to be triggered by anomalous cooling off of Sumatra. We therefore conclude that Pacific ENSO contributes the most to the SIO Rossby wave (up to 64% of the total variance) while the Sumatra contribution is also significant. This conclusion needs to be verified in models.

## 5. Local feedbacks

### a. Atmospheric covariability

Given their well-organized space–time structure, do the aforementioned Rossby wave-induced SST anomalies influence the atmosphere, and does the atmosphere feedback to affect the Rossby wave? The Rossby wave at 10°S takes 2 yr to cross the 70° wide basin,<sup>1</sup> at only 67% of the free Rossby wave speed Chelton et al. (1998) estimated based on the T/P satellite measurements. This

<sup>1</sup> Using low-pass-filtered T/P data for a 6-yr period, White (2000) reports a much slower Rossby wave that crosses the basin in 3.5 yr and suggests that its westward phase propagation is rather constant in speed between 5° and 26°S. Our Z20 correlation with ENSO has a much faster phase speed and does not extend south of 15°S.

slow phase propagation of these interannual Rossby waves may be the first sign for interaction with the atmosphere.

We look into the wind forcing for additional signs of coupling. While its intensification for October–December is probably related to the coupled development of the cold SST and easterly wind anomalies in the equatorial Indian Ocean, the Ekman pumping anomaly remains strong with a tendency to propagate westward with the Rossby wave for a few months (Fig. 11c) after the eastern equatorial SST anomaly dissipates in the following January. From an oceanographic point of view, such a copropagating Ekman pumping resonantly forces the ocean. From a meteorological point of view, it suggests an interaction between surface winds and the Rossby wave.

Significant precipitation anomalies are associated with the Rossby wave-induced SST anomalies. Figure 12a shows the longitude–time section of the 8°–12°S precipitation correlation with the ENSO index for 1979–99 when the CMAP analysis is available. During October–December, the precipitation anomalies show an east–west dipole structure as previously noted by Saji et al. (1999) and Webster et al. (1999). The positive pole in the west extends into East Africa, causing floods (Latif et al. 1999; Reason and Mulenga 1999). During February–August of the following year, positive precipitation correlations of about 0.4–0.6 appear roughly collocated with the downwelling Rossby wave and attendant warm SST anomaly, probably because local SST effects become more important as Pacific ENSO fades away.

Figure 14 shows plan views of SST, wind, and precipitation anomalies for February–May after Pacific ENSO peaks. In February–March, a positive SST anomaly appears in the western equatorial Indian Ocean in response to the arrival of near-equatorial Rossby waves (Murtugudde et al. 2000; Webster et al. 1999). Another positive SST anomaly is centered on 65°E along 8°S, collocated with a positive Z20 anomaly (not shown). An anomalous rainband appears to its south, tilting in a southeast direction. In response, a strong cyclonic circulation develops centered at 25°S, 62°E. The anticyclonic vorticity on the northern edge of this cyclonic circulation maintains the positive Ekman pumping anomaly that sits on and propagates with the SST anomaly in the longitude–time section of Fig. 11c.

With ENSO dissipating in the Pacific by April–May (Fig. 9b), the western SIO warming becomes the dominant feature of the Indian Ocean and anomalous winds appear to be the response to this warming (Fig. 14b). Anomalous winds from the Northern Hemisphere cross the equator to converge onto this southern warming.<sup>2</sup> A

<sup>2</sup> The broad equatorial asymmetry in SST and surface wind anomalies in the boreal spring has been noted by Kawamura et al. (2001) who further suggest that such SST anomalies affect the subsequent summer Asian monsoon.

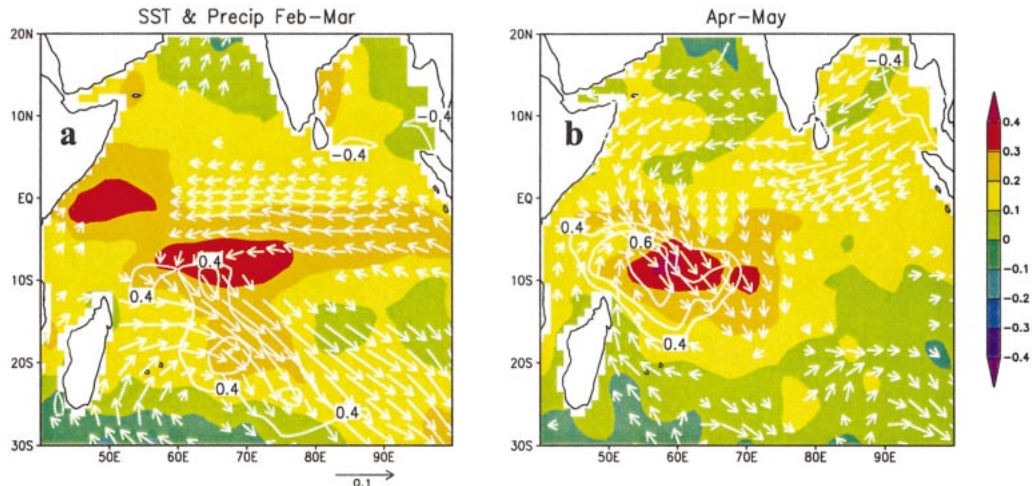


FIG. 14. Regression coefficients of SST (color shade in  $^{\circ}\text{C}$ ) and surface wind stress (vectors in  $10^{-1} \text{ N m}^{-2}$ ) with the ENSO index in (a) Feb–Mar and (b) Apr–May. The precipitation correlation is plotted in contours.

strong positive precipitation anomaly ( $r > 0.6$ ) develops over or slightly west of this positive SST anomaly, exciting a cyclonic circulation in the surface wind. The Ekman upwelling associated with this cyclonic circulation is a negative feedback and acts to dampen the downwelling Rossby wave underneath that causes the western SIO warming in the first place. Theoretical studies have predicted such a negative ocean–atmospheric feedback in an off-equatorial ocean where SST varies in phase with the thermocline depth (Philander et al. 1984; Hirst 1986). This negative feedback and the resultant Ekman upwelling appear responsible for the rapid decay of the Rossby wave after April (Fig. 11c).

Thus, the SIO Rossby wave appears to be coupled with the atmosphere, but the atmospheric feedback changes its sign as the surface cyclonic circulation shifts its position relative to the western SIO warming. Further modeling studies are necessary to determine the cause of this shift. Seasonal variations in the vertical and horizontal shear of the mean atmospheric circulation (e.g., Ting and Yu 1998) and/or remote SST forcing in the

Pacific and other parts of the Indian Ocean may contribute to the wind and precipitation anomalies in February–March that are not confined to the western tropical SIO.

#### b. Tropical cyclones

The tropical SIO is a climatically important region, recording on average 10 named tropical storms/cyclones during the December–April cyclone season. They often bring devastating consequences to islands including highly populated Madagascar. In the 2000 cyclone season, for example, tropical cyclones Eline and Hudah left 800 000 people as disaster victims in Madagascar, a consequence of their heavy rainfall and high winds. Figure 15 shows the number of days per year when named storm/cyclones were observed on a  $4^{\circ} \text{ lat} \times 5^{\circ} \text{ lon}$  grid for 1951–98. The meridional maximum in tropical cyclone days is found along  $15^{\circ}\text{S}$ , and the high-value region enclosed by the 2-cyclone-day per year contour is located just south of the climatological minimum in the thermocline depth where both SST variance and its correlation with the thermocline depth reach maximum (Fig. 1).

To test the hypothesis that the ocean Rossby wave exerts an influence on tropical cyclones through its effect on SST, we make composites of the number of cyclone days when the western tropical SIO ( $8^{\circ}\text{--}12^{\circ}\text{S}$ ,  $50^{\circ}\text{--}70^{\circ}\text{E}$ ) thermocline depth is 0.75 deviation above (below) the normal. There are 10 such deeper-than-normal years and 10 shallower-than-normal years. The deep-year minus shallow-year difference (color shade in Fig. 15) attains a maximum in a region centered about  $66\%$  of the 48-yr mean climatology, indicating that there are 4 cyclone days in a year when the thermocline is abnormally deep as opposed to only 1 in a shallow year.

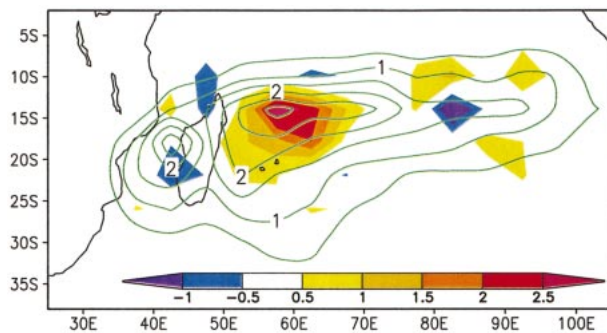


FIG. 15. Climatological-mean tropical cyclone days (contours) in Dec–Apr, and the difference (color shade) between years of anomalously deep and years of anomalously shallow thermocline in  $8^{\circ}\text{--}12^{\circ}\text{S}$ ,  $50^{\circ}\text{--}70^{\circ}\text{E}$ .

This increase in tropical cyclone activity is consistent with the anomalous cyclonic circulation in the lower atmosphere depicted in Fig. 14.

Composites based on SST in the same western tropical SIO region yield similar results (not shown). Jury et al. (1999) note a similar SST–cyclone correlation and find that empirical prediction of tropical cyclone days using the WTSIO SST as a predictor yields useful skill. Our analysis shows that the subsurface Rossby wave is the major cause of this key SST variability. The slow phase propagation of this Rossby wave therefore provides useful predictability for SST and tropical cyclone forecasts.

## 6. Other regions

So far, we have focused on the SIO Rossby wave, its forcing and interaction with the atmosphere. Now, we turn our attention to other regional aspects of SIO climate variability; namely, the Indonesian coast and the southeastern subtropics.

### a. Java upwelling

The anomalous easterlies in the equatorial Indian Ocean during a positive event of ENSO help raise the thermocline in the eastern ocean, thereby enhancing the thermocline feedback on SST. Significant ENSO-related equatorial easterlies, however, develop only during and after the Sumatra cooling event (Fig. 9b). Since the eastern Indian Ocean cooling starts from the coast of Sumatra (Saji et al. 1999; Murtugudde et al. 2000), here we take a close look at the time evolution of SST anomalies along the Indonesian coast. For this purpose, we use the satellite/in situ blended SST measurements<sup>3</sup> to construct a dataset along the coast rather than SODA, because the 1° horizontal resolution in SODA does not adequately resolve the coastal processes and introduces some noise. Features from the SODA analysis, however, are qualitatively similar.

A moderate cooling off the Java coast (105°–116°E) begins in March between Java and Timor, Indonesia, then shifts northwestward along the coast, finally reaching Sumatra 2–3 months later in May–June (Fig. 16). There, it amplifies and spreads over a large area of the eastern equatorial Indian Ocean. As Webster et al. (1999) and Murtugudde et al. (2000) suggested, a negative thermocline depth anomaly appears to come from the west along the equator and reach the Sumatra coast in April 1997. It is tempting to suggest that the former triggers the coastal cooling, but this hypothesis is inconsistent with our analysis in Fig. 16. High SST correlation (>0.6) first appears on eastern Java in March,

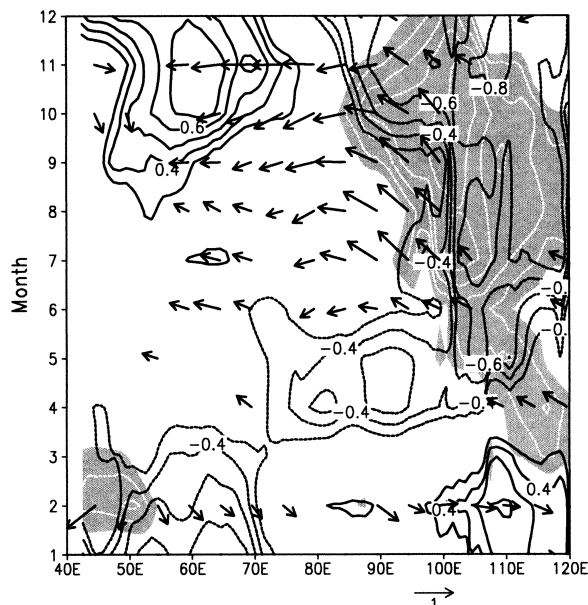


FIG. 16. Lagged correlations with the Sumatra index of SST (shade  $< -0.4$  with 0.1 contour intervals), Z20 (contours), and wind stress (vectors) as a function of distance and calendar month. The sign is reversed. The horizontal axis is the lon along the equator west of 97°E, then turns southeast and follows the Indonesian coast. Along-shore along-equator winds appear horizontal.

one month before the Z20 anomaly reaches Sumatra. The northwestward propagation and amplification of SST correlation along the coast (Fig. 16) is against the direction of a coastal Kelvin, but in the same direction as the seasonal onset of upwelling-favorable coastal winds (Fig. 2). Consistent with this result, Murtugudde et al. (2000) concluded that the Sumatra cooling in their model solution was due equally to local and remote (equatorial) forcing.

### b. Subtropical SIO warming

The eastern subtropical SIO is another region where SST shows significant correlation with both ENSO and Sumatra variability. Figure 17 displays the correlations between the Sumatra index and SST and wind stress averaged for 25°–30°S. Toward the end of a Sumatra cooling event, anomalous northwesterlies appear in the eastern subtropical SIO (Fig. 17; see Fig. 10 for a basin-scale plan view). These anomalous winds weaken the prevailing climatological southeasterlies and hence reduce the latent and sensible heat release from the sea surface, leading to a strong warming that peaks in January and persists for another two or three months. Yu and Rienecker (1999) noted such a subtropical warming in the 1997–98 austral summer. An ocean-model simulation also indicates the important role played by local heat flux in forcing SST variability in this region (Behara et al. 2000). Consistent with this view, the SST correlation is rather stationary, without any obvious zon-

<sup>3</sup> Located within an active atmospheric convection center, the eastern equatorial Indian Ocean is often covered by high clouds, which may render infrared SST measurements ineffective. Further validation with new microwave remote-sensing measurements is necessary.

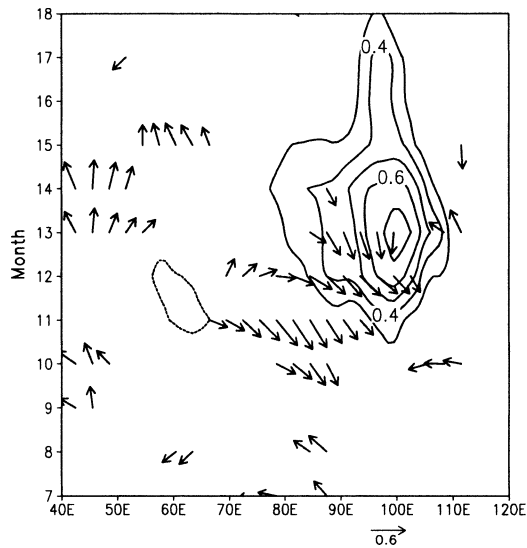


FIG. 17. Lagged correlations of SST (contours) and wind stress (vectors), averaged in  $25^{\circ}$ – $30^{\circ}$ S, with the Sumatra index as a function of lon and calendar month. The sign is reversed.

al propagation (Fig. 17). Furthermore, no significant covariability is found in the thermocline depth (not shown), in contrast to the tropical SIO. Near  $25^{\circ}$ S,  $100^{\circ}$ E, the Z18–SST correlation is noisy and not well organized in the IX-12 XBT section and is insignificant in SODA (Fig. 4). Ocean Rossby waves are observed at  $25^{\circ}$ S (Birol and Morrow 2001), but do not appear to be a major cause of SST variability there.

Unlike the SST variability in the western tropical SIO discussed in section 4, SST in this subtropical region correlates better with the Sumatra index than with ENSO (maximum value 0.7 vs 0.5). This appears to suggest that Sumatra SST variability excites atmospheric waves that pass over this subtropical region and generate SST variability there in local summer, but an AGCM mixed-layer coupled model that is forced by observed equatorial Pacific SST variations reproduces this subtropical SIO SST variability quantitatively well (ABNLLS). Carefully designed GCM experiments are needed to better understand ENSO and Sumatra teleconnection mechanisms.

Because of the seasonality of Sumatra variability and ENSO, their teleconnection effect on subtropical SIO SST is limited to the austral summer.<sup>4</sup> So again, data stratification by calendar month is a key to obtaining significant correlation with either Sumatra variability or ENSO. Without seasonal stratification, the simultaneous correlation of SST in the southeastern subtropics ( $25^{\circ}$ – $30^{\circ}$ S,  $95^{\circ}$ – $105^{\circ}$ E) falls below meaningful significance levels—to 0.14 with Sumatra and 0.19 with eastern Pacific SST—consistent with the results of Behera and Yamagata (2001).

<sup>4</sup> It is unclear what causes SST variability in austral winter, which is related to rainfall anomalies over Australia (Nicholls 1989).

## 7. Summary and discussion

We have studied the time–space structure and mechanisms of interannual variability in the SIO, using a variety of datasets that include in situ and satellite measurements and model-based data assimilation products. Because SIO variability is strongly phase locked to the seasonal cycle, all the statistics cited here are based on data stratified by calendar month. Consistent with previous studies (Nigam and Shen 1993; Klein et al. 1999; Lau and Nath 2000), we find that SST variability over the Indian Ocean, including the region off Sumatra, correlates significantly with Pacific ENSO. Moreover, the SST correlation is significantly higher with Pacific ENSO than with Sumatra variability except in the eastern subtropical SIO and (trivially) the eastern equatorial Indian Ocean.

Based on a high correlation between thermocline depth and SST, we identify the western tropical SIO centered at  $10^{\circ}$ S as a region where subsurface ocean dynamics impacts SST variability and thereby the atmosphere. This ocean dynamic effect can explain the discrepancy Klein et al. (1999) found between SST and surface heat flux variability in this region. During a positive ENSO event, curl associated with the anomalous equatorial easterlies force a downwelling Rossby wave with maximum amplitude around  $10^{\circ}$ S. A positive SST anomaly is found to copropagate with this Rossby wave, strongly indicating a subsurface-to-surface feedback. Over such a westward-traveling SST anomaly, anomalous meridional winds are consistently northerly while zonal winds change its direction, suggesting that local heat flux and Ekman drift effects are small.

While it is forced by ENSO and Sumatra variability to the lowest order, we present evidence that this Rossby wave interacts with the atmosphere. At the developing stage of this Rossby wave, Ekman pumping appears to contain an in-phase westward-propagating component, exerting a resonant forcing. We also detect a significant increase in tropical cyclone activity associated with the resultant SST warming in the western SIO. By April, after the thermocline depth anomaly reaches maximum amplitude, a positive precipitation anomaly and a cyclonic surface circulation are collocated with the thermocline depth and SST anomaly, and their interaction is a negative feedback that quickly dampens the Rossby wave. The relative location of the cyclonic circulation response to the Rossby wave–induced SST anomaly appears to be the key to the sign of atmospheric feedback. Whether and how such a change in their relative position takes place needs to be investigated with models.

The Indian Ocean is the only ocean with climatological westerly winds on the equator. The shear between these westerlies and the southeasterly trades results in an open-ocean upwelling band from  $5^{\circ}$  to  $15^{\circ}$ S, raising the thermocline in the western tropical SIO. This upwelling sets favorable conditions for the subsurface Rossby wave to interact with the atmosphere. Rossby

waves are at the heart of all theories of ENSO and equatorial interannual variability, providing the crucial memory (Neelin et al. 1998). In the Pacific and Atlantic, tropical Rossby waves hide in the deep thermocline on their way to the west with little signature in SST, and hence they are undetected by the atmosphere<sup>5</sup> (Neelin et al. 1998). In the western SIO, by contrast, the thermocline is shallow and Rossby waves cause significant SST anomalies that can interact with the atmosphere. It is thus conceivable that the coupled nature of the SIO Rossby waves may play an important role in shaping tropical Indian Ocean climate and its variability. Indeed, coupled ocean–atmosphere models where oceanic Rossby waves propagate freely (Xie et al. 1989) behave very differently from those where these waves are strongly damped by air–sea interaction (Anderson and McCreary 1985).

Given the deep climatological thermocline on the equator and Indonesian coast, it is somewhat surprising that the Bjerknes feedback operates at all in the Indian Ocean. But because SST in the eastern Indian Ocean is normally high, where strong atmospheric convection takes place, a modest SST anomaly there can induce a large atmospheric response. This strong atmospheric feedback allows the coupled anomalies to grow into large amplitudes—SST anomalies exceed 3°C off Sumatra in the 1997 cold event—despite the weak thermocline feedback along the equator. In the equatorial Pacific and Atlantic, in comparison, the thermocline feedback is strong in the east but the cold climatological SST there limits atmospheric feedback (see Xie et al. 1999 for a comparative study of the tropical Pacific and Atlantic).

Together with several recent studies (Murtugudde et al. 2000; Saji et al. 1999; Webster et al. 1999; Behera et al. 2000), our analysis paints an Indian Ocean where ocean dynamics, namely Sumatra upwelling and the SIO Rossby wave, play a more important role than previously thought. This more dynamic view of the Indian Ocean implies potentially useful predictability for western SIO climate variability. Figure 11a shows that with the input of the eastern equatorial Pacific SST by December, 64% of the total thermocline depth variance in the western SIO (8°–12°S, 60°–70°E) in spring can be predicted more than 3 months ahead. This simple scheme can be further improved by adding a prediction model for Pacific ENSO. In addition, SST off eastern Java may be used as a statistical precursor for predicting Sumatra variability, which affects regional climate along the equator. Whether and how these potential predictabilities can be realized needs further studies with improved coupled models, but a prediction model that includes upwelling, Rossby waves, and other ocean dynamics, will almost certainly improve Indian Ocean climate prediction.

<sup>5</sup> Recently, this uncoupled view for Pacific Rossby waves is being questioned (Wang et al. 1999).

*Acknowledgments.* We thank G. Meyers for providing the XBT data, J. Hafner and Y. Shen of IPRC and R. Schoenefeldt of IfM Kiel for data processing, and A. R. Subbiah and M. Rakotondratara for information on SIO cyclone disasters. Supported by the Frontier Research System for Global Change and NASA under Grant NAG5-10045 and JPL Contract 1216010.

#### REFERENCES

- Anderson, D. L. T., and J. P. McCreary, 1985: Slowly propagating disturbances in a coupled ocean–atmosphere model. *J. Atmos. Sci.*, **42**, 615–629.
- Behera, S. K., and T. Yamagata, 2001: Subtropical SST dipole events in the southern Indian Ocean. *Geophys. Res. Lett.*, **28**, 327–330.
- , P. S. Salvekar, and T. Yamagata, 2000: Simulation of interannual SST variability in the tropical Indian Ocean. *J. Climate*, **13**, 3487–3499.
- Birol, F., and R. Morrow, 2001: Sources of the baroclinic waves in the southeast Indian Ocean. *J. Geophys. Res.*, **106**, 9145–9160.
- Bjerknes, J., 1969: Atmospheric teleconnections from the equatorial Pacific. *Mon. Wea. Rev.*, **97**, 163–172.
- Carton, J. A., G. Chepurin, X. Cao, and B. Giese, 2000: A simple ocean data assimilation analysis of the global upper ocean 1950–95. Part I: Methodology. *J. Phys. Oceanogr.*, **30**, 294–309.
- Chambers, D. P., B. D. Tapley, and R. H. Stewart, 1999: Anomalous warming in the Indian Ocean coincident with El Niño. *J. Geophys. Res.*, **104**, 3035–3047.
- Chelton, D. B., R. A. de Szoeke, M. G. Schlax, K. El Naggar, and N. Siwertz, 1998: Geographic variability of the first baroclinic Rossby radius of deformation. *J. Phys. Oceanogr.*, **28**, 433–460.
- da Silva, A. M., C. C. Young, and S. Levitus, 1994: *Atlas of Surface Marine Data 1994*. NOAA Atlas NESDIS 6, 83 pp.
- Godfrey, J. S., 1996: The effect of the Indonesian Throughflow on ocean circulation and heat exchange with the atmosphere: A review. *J. Geophys. Res.*, **101**, 12 217–12 237.
- Hirst, A. C., 1986: Unstable and damped equatorial modes in simple coupled ocean–atmosphere models. *J. Atmos. Sci.*, **43**, 606–630.
- Huang, B., and J. L. Kinter, 2001: The interannual variability in the tropical Indian Ocean and its relations to El Niño/Southern Oscillation. Center for Ocean–Land–Atmosphere Studies. Tech. Rep. 94, Calverton, MD, 48 pp.
- Iizuka, S., T. Matsuura, and T. Yamagata, 2000: The Indian Ocean SST dipole simulated in a coupled general circulation model. *Geophys. Res. Lett.*, **27**, 3369–3372.
- Jury, M. R., B. Pathack, and B. Parker, 1999: Climatic determinants and statistical prediction of tropical cyclone days in the southwest Indian Ocean. *J. Climate*, **12**, 1738–1746.
- Kalnay, E., and Coauthors, 1996: The NCEP/NCAR 40-Year Reanalysis Project. *Bull. Amer. Meteor. Soc.*, **77**, 437–471.
- Kawamura, R., T. Matsumura, and S. Iizuka, 2001: Role of equatorially asymmetric sea surface temperature anomalies in the Indian Ocean in the Asian summer monsoon and El Niño–Southern Oscillation coupling. *J. Geophys. Res.*, **106**, 4681–4693.
- Klein, S. A., B. J. Soden, and N.-C. Lau, 1999: Remote sea surface temperature variations during ENSO: Evidence for a tropical atmospheric bridge. *J. Climate*, **12**, 917–932.
- Latif, M., and T. P. Barnett, 1995: Interactions of the tropical oceans. *J. Climate*, **8**, 952–964.
- , D. Dommengat, M. Dima, and A. Grotzner, 1999: The role of Indian Ocean sea surface temperature in forcing east African rainfall anomalies during December–January 1997/98. *J. Climate*, **12**, 3497–3504.
- Lau, N.-C., and M. J. Nath, 2000: Impact of ENSO on the variability of the Asian–Australian monsoons as simulated in GCM experiments. *J. Climate*, **13**, 4287–4309.
- Masumoto, Y., and G. Meyers, 1998: Forced Rossby waves in the

- southern tropical Indian Ocean. *J. Geophys. Res.*, **103**, 27 589–27 602.
- Meyers, G., 1996: Variation of Indonesian throughflow and the El Niño–Southern Oscillation. *J. Geophys. Res.*, **101**, 12 255–12 263.
- Mitchell, T., cited 2001: Tropical cyclone positions. [Available online at [http://tao.atmos.washington.edu/data\\_sets/tropical\\_cyclones/#data](http://tao.atmos.washington.edu/data_sets/tropical_cyclones/#data).]
- Murtugudde, R., and A. J. Busalacchi, 1999: Interannual variability of the dynamics and thermodynamics, and mixed layer processes in the Indian Ocean. *J. Climate*, **12**, 2300–2326.
- , S. Signorini, J. Christian, A. Busalacchi, and C. McClain, 1999: Ocean color variability of the tropical Indo-Pacific basin observed by SeaWiFS during 1997–98. *J. Geophys. Res.*, **104**, 18 351–18 366.
- , J. P. McCreary, and A. J. Busalacchi, 2000: Oceanic processes associated with anomalous events in the Indian Ocean with relevance to 1997–1998. *J. Geophys. Res.*, **105**, 3295–3306.
- Neelin, J. D., D. S. Battisti, A. C. Hirst, F.-F. Jin, Y. Wakata, T. Yamagata, and S. E. Zebiak, 1998: ENSO theory. *J. Geophys. Res.*, **103**, 14 261–14 290.
- Nicholls, N., 1989: Sea surface temperature and Australian winter rainfall. *J. Climate*, **2**, 965–973.
- Nigam, S., and H. S. Shen, 1993: Structure of oceanic and atmospheric low-frequency variability over the tropical Pacific and Indian Oceans. Part I: COADS observations. *J. Climate*, **6**, 657–676.
- Perigaud, C., and P. Delecluse, 1993: Interannual sea level variations in the tropical Indian Ocean from Geosat and shallow water simulations. *J. Phys. Oceanogr.*, **23**, 1916–1934.
- Philander, S. G. H., T. Yamagata, and R. C. Pacanowski, 1984: Unstable air–sea interactions in the Tropics. *J. Atmos. Sci.*, **41**, 604–613.
- Pigot, L., and G. Meyers, 1999: Analysis of frequently repeated XBT lines in the Indian Ocean. CSIRO Marine Lab. Rep. 238, Hobart, Australia, 43 pp. [Available online at <http://www.marine.csiro.au/~pigot/REPORT/overview.html>.]
- Reason, C. J. C., and H. M. Mulenga, 1999: Relationships between South African rainfall and SST anomalies in the SW Indian Ocean. *Int. J. Climatol.*, **19**, 1651–1673.
- Reverdin, G., D. Cadel, and D. Gutzler, 1986: Interannual displacements of convection and surface circulation over the equatorial Indian Ocean. *Quart. J. Roy. Meteor. Soc.*, **112**, 43–67.
- Reynolds, R. W., and T. M. Smith, 1994: Improved global sea surface temperature analyses using optimal interpolation. *J. Climate*, **7**, 929–948.
- Saji, N. H., B. N. Goswami, P. N. Vinayachandran, and T. Yamagata, 1999: A dipole mode in the tropical Indian Ocean. *Nature*, **401**, 360–363.
- Schiller, A., J. S. Godfrey, P. C. McIntosh, G. Meyers, and R. Fielder, 2000: Interannual dynamics and thermodynamics of the Indo-Pacific Oceans. *J. Phys. Oceanogr.*, **30**, 987–1012.
- Schott, F. A., and J. P. McCreary, 2001: The monsoon circulation of the Indian Ocean. *Progress in Oceanography*, Pergamon, in press.
- Slingo, J. M., and H. Annamalai, 2000: 1997: The El Niño of the century and the response of the Indian summer monsoon. *Mon. Wea. Rev.*, **128**, 1778–1797.
- Ting, M., and L. Yu, 1998: Steady response to tropical heating in wavy linear and nonlinear baroclinic models. *J. Atmos. Sci.*, **55**, 3565–3582.
- Trenberth, K. E., G. W. Branstator, D. Karoly, A. Kumar, N.-C. Lau, and C. Ropelewski, 1998: Progress during TOGA in understanding and modeling global teleconnections associated with tropical sea surface temperatures. *J. Geophys. Res.*, **103**, 14 291–14 324.
- Ueda, H., and J. Matsumoto, 2000: A possible triggering process of east–west asymmetric anomalies over the Indian Ocean in relation to 1997/98 El Niño. *J. Meteor. Soc. Japan*, **78**, 803–818.
- Wallace, J. M., E. M. Rasmusson, T. P. Mitchell, V. E. Kousky, E. S. Sarachik, and H. von Storch, 1998: On the structure and evolution of ENSO-related climate variability in the tropical Pacific: Lessons from TOGA. *J. Geophys. Res.*, **103**, 14 241–14 259.
- Wang, C., R. H. Weisberg, and J. I. Virmani, 1999: Western Pacific interannual variability associated with the El Niño–Southern Oscillation. *J. Geophys. Res.*, **104**, 5131–5149.
- Webster, P. J., A. M. Moore, J. P. Loschnigg, and R. R. Leben, 1999: Coupled oceanic–atmospheric dynamics in the Indian Ocean during 1997–98. *Nature*, **401**, 356–360.
- White, W. B., 2000: Coupled Rossby waves in the Indian Ocean on interannual timescales. *J. Phys. Oceanogr.*, **30**, 2972–2988.
- Xie, P., and P. A. Arkin, 1996: Analyses of global monthly precipitation using gauge observations, satellite estimates, and numerical model predictions. *J. Climate*, **9**, 840–858.
- Xie, S.-P., A. Kubokawa, and K. Hanawa, 1989: Oscillations with two feedback processes in a coupled ocean–atmosphere model. *J. Climate*, **2**, 946–964.
- , Y. Tanimoto, H. Noguchi, and T. Matsuno, 1999: How and why climate variability differs between the tropical Pacific and Atlantic. *Geophys. Res. Lett.*, **26**, 1609–1612.
- Yu, L. S., and M. M. Rienecker, 1999: Mechanisms for the Indian Ocean warming during the 1997–98 El Niño. *Geophys. Res. Lett.*, **26**, 735–738.